

Operator relaxation and the optimal depth of classical shadows

Matteo Ippoliti, Yaodong Li, Tibor Rakovszky, and Vedika Khemani
Department of Physics, Stanford University, Stanford, CA 94305, USA

Classical shadows are a powerful method for learning many properties of quantum states in a sample-efficient manner, by making use of randomized measurements. Here we study the sample complexity of learning the expectation value of Pauli operators via “shallow shadows”, a recently-proposed version of classical shadows in which the randomization step is effected by a local unitary circuit of variable depth t . We show that the state-averaged shadow norm (the quantity controlling the average sample complexity) is expressed in terms of properties of the Heisenberg time evolution of operators under the randomizing (“twirling”) circuit—namely the evolution of the *weight distribution* characterizing the number of sites on which an operator acts nontrivially. For spatially-contiguous operators of weight k , this entails a competition between two processes: *operator spreading* (whereby the support of an operator grows over time, increasing its weight) and *operator relaxation* (whereby the bulk of the operator develops an equilibrium density of identity operators, decreasing its weight). From this simple picture we derive (i) an upper bound on the shadow norm which, for depth $t \sim \log(k)$, guarantees an exponential gain in sample complexity over the $t = 0$ protocol in any spatial dimension, and (ii) quantitative results in one dimension within a mean-field approximation, including a universal subleading correction to the optimal depth, found to be in excellent agreement with infinite matrix product state numerical simulations. Our work connects fundamental ideas in quantum many-body dynamics to applications in quantum information science, and paves the way to highly-optimized protocols for learning different properties of quantum states.

Introduction. The development of controllable quantum simulators has enabled the creation of complex and highly entangled quantum states in laboratory settings, leading to exciting new developments in quantum information science and many-body physics [1–8]. These advances raise the issue of how to efficiently characterize such complex quantum states. Full quantum state tomography requires a number of measurements that scales exponentially in the size of the system [9], motivating the need for more scalable and efficient state-learning protocols. Recent progress in this direction has come from the development of *classical shadows* [10–21], a method to extract many physical properties of states with a dramatically smaller number of measurements. In this work, we shed light on the inner workings of classical shadows by making connections to foundational ideas in quantum dynamics on the spreading and equilibration of operators.

Classical shadows use *randomized measurements* [22–24] to form a compact representation of the many-body quantum state of interest. The state ρ is first transformed by a random unitary operation U (chosen from a suitable “twirling ensemble”), and then projectively measured, yielding a computational basis state $|b\rangle$. The measured basis state is then rotated backwards (on a classical computer) to yield a “snapshot”, $\hat{\sigma}_{U,b} = U^\dagger |b\rangle\langle b| U$. The average of these snapshots (over choices of the twirling unitary and measurement outcomes) is related to the true state ρ by a quantum channel, $\mathbb{E}_{U,b}[\hat{\sigma}_{U,b}] = \mathcal{M}(\rho)$. If the measurements are *tomographically complete* [11], the channel \mathcal{M} can be inverted (again on a classical computer) to produce “inverted snapshots” $\hat{\rho}_{U,b} = \mathcal{M}^{-1}(\hat{\sigma}_{U,b})$. These form a compact, approximate description of the quantum state ρ —its *classical shadow* [11]. This protocol is sketched in Fig. 1(a). From

this description one can then extract many properties of the state. Remarkably, the randomization ensures that the properties do not have to be specified in advance—the general philosophy of the method is to “*measure first, ask questions later*” [24].

A key practical consideration for the usefulness of classical shadows is their *sample complexity*, i.e., the number of experimental samples needed in order to estimate a certain property of ρ to within a given error. To learn an expectation value $\text{Tr}(\rho O)$, one builds estimators $\hat{o}_{U,b} = \text{Tr}(\hat{\rho}_{U,b} O)$ that yield the desired value in expectation ($\mathbb{E}_{U,b}[\hat{o}_{U,b}] = \text{Tr}(\rho O)$). The sample complexity is determined by the scaling of the variance of \hat{o} , captured by the *shadow norm* $\|O\|_{\text{sh}}$, itself a function of the twirling ensemble. The freedom in choosing the twirling ensemble can thus be leveraged to optimize the learnability of certain properties of a quantum state. For instance, “local twirling” (where $U = \bigotimes_i u_i$ is a product of single-qubit random unitaries) gives $\|O\|_{\text{sh}}^2 = 3^k$, where k is the number of qubits on which O acts nontrivially; this is best suited to learning the value of few-body operators, but poorly suited to learning global properties of ρ . On the opposite end, “global twirling” (where U is a random Clifford unitary on the whole Hilbert space) gives $\|O\|_{\text{sh}}^2 = \text{Tr}(O^\dagger O)$, which favors learning e.g. the fidelity with a pure many-body state $O = |\psi\rangle\langle\psi|$, but performs poorly on Pauli operators ($\|O\|_{\text{sh}}^2 = 2^N$) irrespective of locality [11].

Intermediate schemes, dubbed *shallow shadows*, have been recently proposed [25–27] and use twirling ensembles made of shallow quantum circuits, whose depth t can be tuned to interpolate between the local and global twirling limits. These are easier to implement on near-term quantum hardware as compared to global unitaries. Further, the finite depth t enables the efficient classi-

cal computation of $\hat{\sigma}$ and $\hat{\rho}$ via tensor-network methods [25, 26]. Surprisingly, these schemes were numerically observed to perform better than local twirling for the problem of estimating the expectation value of contiguous, multi-site Pauli operators (interesting examples of such operators include string order parameters for characterizing topological phases [28, 29] and check operators of a quantum code [30]). The optimal depth $t^*(k)$ for a Pauli operator acting on k contiguous sites was observed numerically to scale as $\text{polylog}(k)$ in one dimension [25], with a significant gain in sample complexity over the local twirling protocol. The physical mechanism behind this behavior has remained elusive thus far.

Here we analyze this problem analytically and find a mapping of the shadow norm to the dynamics of *Hamming weight* (the number of sites on which a Pauli operator acts nontrivially, henceforth just ‘weight’) under the twirling evolution. This mapping reveals that the optimal depth for the estimation of contiguous Pauli operators is determined by the competition of two processes under chaotic unitary dynamics, sketched in Fig. 1(b): *operator spreading* [31–36] and *operator relaxation*, to be defined below. Based on this picture, we prove that at depth $t^*(k) \sim \log(k)$, shallow shadows realize an exponential-in- k gain in sample complexity over local twirling in any finite spatial dimension. We further develop an analytical mean-field approximation for the (state-averaged) shadow norm in one dimension, indicating that at depth $t^*(k)$ the sample complexity nearly saturates a lower bound ($\sim 2^k$, up to $\text{poly}(k)$ corrections), as sketched in Fig. 1(c); the prediction shows excellent agreement with numerics on large Pauli operators (up to $k = 1000$) in infinite 1D systems. We also argue that the optimal depth is zero (i.e. local twirling is optimal) in non-local models, e.g. on complete graphs, or if the Pauli operators to be learned are k -local but not geometrically local.

Our results shed light on the inner workings of the classical shadows protocol and how it relates to fundamental aspects of quantum dynamics. At the same time, they give a practical, operational meaning to ideas about chaotic operator dynamics, and promise applications towards highly optimized classical shadows protocols for near-term quantum devices.

Shadow norm and operator weight. We begin by deriving a general relationship between the shadow norm and operator dynamics which holds for any twirling ensemble that is *locally scrambled* [37, 38], i.e., such that measure dU over the ensemble is invariant under $U \mapsto VU$ and $U \mapsto UV$ for all product Clifford unitaries [39] $V = \bigotimes_i v_i$, $v_i \in \text{Cliff}(q)$ (this holds for the case of local and global twirling, as well as for shallow shadows in Refs. [25, 26]).

We will consider a system of q -state qudits arranged on a d -dimensional lattice consisting of N qudits. For qudits with $q > 2$, we use “generalized Pauli operators” defined by products of clock and shift unitary operators [40]. The

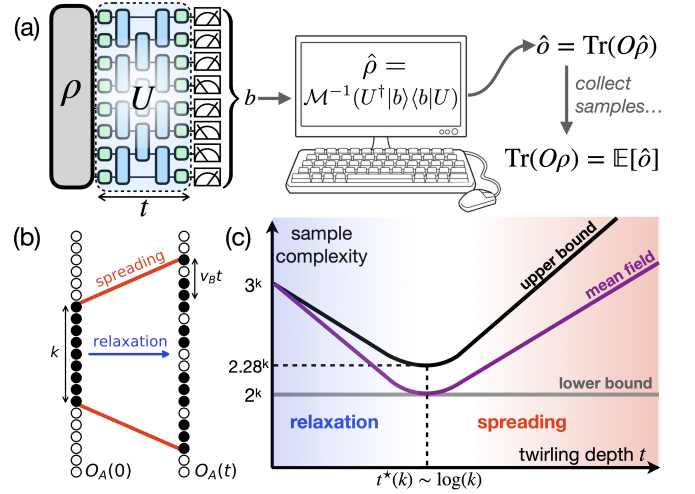


FIG. 1. (a) Schematic of classical shadows via shallow circuits: a state ρ is randomized by a “twirling” circuit U of depth t , then measured; data is classically processed to estimate Pauli expectation values. (b) Operator spreading and relaxation under chaotic dynamics. \circ/\bullet denote identity and traceless Pauli matrices, respectively. $O_A(0)$ is a contiguous Pauli operator of weight k . $O_A(t)$ may be a superposition of many Pauli operators; a typical one is shown. (c) Summary of main results of this work. The competition between operator spreading and relaxation determines the optimal sample complexity of learning Pauli expectation values with this protocol.

measurement channel reads

$$\mathcal{M}(\rho) = \sum_b \int dU \underbrace{\langle b|U\rho U^\dagger|b\rangle}_{\text{Prob}(b|\rho,U)} \underbrace{U^\dagger|b\rangle\langle b|U}_{\text{snapshot } \hat{\sigma}_{U,b}}, \quad (1)$$

where b ranges over all $D = q^N$ computational basis states.

All Pauli operators are eigenmodes of the channel [25, 26], and the eigenvalue depends solely on the twirling ensemble and on the subsystem A on which the Pauli operator is supported: $\mathcal{M}[O_A] = \lambda_A O_A$, where O_A denotes a Pauli operator supported in a region A . The eigenvalues can be expressed as [41]

$$\lambda_A = \sum_{w=1}^N \pi_{A,t}(w) (q+1)^{-w}, \quad (2)$$

where $\pi_{A,t}(w)$ is the averaged *weight distribution* of the twirled operator $O_A(t) \equiv U O_A U^\dagger$:

$$\pi_{A,t}(w) = \sum_{P: |P|=w} \mathbb{E}_U |D^{-1} \text{Tr}(P O_A(t))|^2. \quad (3)$$

Here the sum runs over Pauli operators P , and $|P|$ is the weight of P .

With this result, we can exactly compute the *state-averaged shadow norm* [42], henceforth referred to as

‘shadow norm’: $\|O_A\|_{\text{sh,avg}}^2 = \text{Tr}(O_A \mathcal{M}^{-1}[O_A])/D = \lambda_A^{-1}$ [26, 41]. Combined with the expression for λ_A in Eq. (2), this yields an exact relationship between the shadow norm and the weight distribution of a twirled operator,

$$\|O_A\|_{\text{sh,avg}}^2 = \left[\overline{(q+1)^{-w}} \right]^{-1} \quad (4)$$

where the overline denotes averaging over w according to $\pi_{A,t}(w)$. Eq. (4) constitutes one of the main results of our work.

It is straightforward to verify that Eq. (4) reproduces the well-known results for local and global twirling of qubits (3^k and 2^N respectively [11]) in the $t = 0$ and $t \rightarrow \infty$ limits [41]. However, our result allows us to understand the behavior of the shadow norm away from these well-known limits, by leveraging the connection to the dynamics of operator weight under chaotic evolution (i.e. the twirling ensemble U) as a function of time (i.e. the variable depth t).

Relaxation of operator weight. In the following we focus on Pauli operators whose support A is a spatially-contiguous region, and consider twirling ensembles of *diluted* random brickwork circuits, i.e. circuits where each gate is sampled from the Haar measure on $U(q^2)$ with probability ϵ and is the identity otherwise. These include conventional random circuits ($\epsilon = 1$), but allow us to slow down the twirling dynamics, effectively providing a finer discretization of time, which will prove useful below. To study the dynamics of operator weight during the twirling, let us introduce “occupation” variables n_i , where $n_i = 0$ if a Pauli operator is the identity at site i , and $n_i = 1$ otherwise. Before twirling, we have a *fully-packed* Pauli operator in region A : $n_i = 1$ iff $i \in A$. As the twirling depth t increases, two things happen: (i) *Operator spreading*—the boundary of the operator moves outwards, so that $\bar{n}_i(t) > 0$ also on sites $i \notin A$ that were initially empty, leading to an *increase* in weight; and (ii) *Operator relaxation*—the bulk of the operator relaxes from its fully-packed initial state ($n_i = 1 \forall i \in A$) towards an equilibrium density $\bar{n}_i(t) \rightarrow 1 - q^{-2}$ (when all q^2 Pauli operators are equally likely), leading to a *decrease* in weight.

As the latter is a bulk effect, it always dominates (at early times) for a sufficiently large region A . Thus the shadow norm must initially decrease from its $t = 0$ value (local twirling), before eventually becoming dominated by operator spreading and increasing again towards its $t \rightarrow \infty$ value (global twirling), implying a minimum at some finite optimal depth t^* .

To characterize the relaxation process, let us start by focusing on an infinite, fully-packed Pauli operator, and consider the average occupation of a site $\bar{n}_i(t)$ as a function of twirling depth t . For the twirling ensembles under consideration (brickwork circuits of Haar-random gates, possibly diluted) this problem can be addressed analytically in one spatial dimension. We can leverage earlier results [33, 35] to show that the vector of oc-

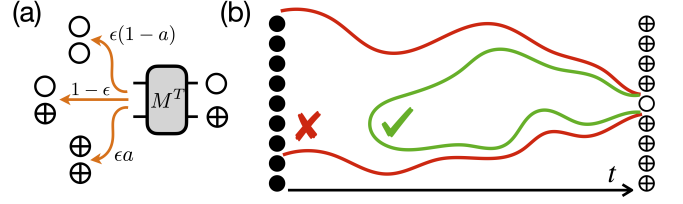


FIG. 2. Random-walk calculation of Pauli density relaxation. (a) Update rules for a domain wall between \oplus and \circ states. (b) Schematic of the random-walk calculation for the average density of holes $\bar{h}_i(t)$: if the two walkers fail to annihilate within t steps, the diagram vanishes.

cupation probabilities $p_{\mathbf{n}}$ (where $\mathbf{n} \in \{0, 1\}^N$ labels occupation configurations) evolves according to a Markov process, $p'_{\mathbf{n}} = \sum_{\mathbf{m}} \mathbb{M}_{\mathbf{n},\mathbf{m}} p_{\mathbf{m}}$, with \mathbb{M} a stochastic matrix ($\sum_{\mathbf{m}} \mathbb{M}_{\mathbf{m},\mathbf{n}} = 1 \forall \mathbf{n}$), and solve for the local occupation number analytically.

For convenience, we focus on the “density of holes” \bar{h}_i ($h_i \equiv 1 - n_i$) and we introduce on-site vectors in the binary space of (identity, traceless Pauli): $|\bullet\rangle = (0, 1)^T$, $|\circ\rangle = (1, 0)^T$ and $|\oplus\rangle = (1, 1)^T$. The calculation involves a fully-packed initial state $p_{\mathbf{n}}^{\text{init}} = \prod_i \delta_{n_i, 1}$, evolved under the averaged brickwork circuit giving a final state $p_{\mathbf{n}}^{\text{final}}$; we are then interested in $\bar{h}_i = \sum_{\mathbf{n}} p_{\mathbf{n}}^{\text{final}} \delta_{n_i, 0}$. This corresponds to a matrix element $(\cdots \oplus \oplus \circ \oplus \oplus \cdots | \mathbb{M}_t | \cdots \bullet \bullet \bullet \cdots)$ where \mathbb{M}_t is the transition matrix for the averaged depth- t twirling circuit.

It is advantageous to consider the *backward* evolution \mathbb{M}_t^T acting on the state $|\cdots \oplus \oplus \oplus \oplus \oplus \cdots\rangle$: as illustrated in Fig. 2(a), we have $M^T |\oplus \oplus\rangle = \epsilon a |\oplus \oplus\rangle + (1 - \epsilon) |\oplus \oplus\rangle + \epsilon(1 - a) |\circ \circ\rangle$, where M is the transition matrix for a single two-qudit gate, $a = 1/(q^2 + 1)$, and ϵ is the dilution parameter (see [41]). Moreover it follows from unitarity that $M^T |\oplus \oplus\rangle = |\oplus \oplus\rangle$ and $M^T |\circ \circ\rangle = |\circ \circ\rangle$. Thus the structure of a domain of \circ in a background of \oplus is preserved under the backward evolution, and domain walls undergo a random walk with a bias that tends to expand the \circ domain. When the domain walls are adjacent, they may annihilate, leading to an all- \oplus state which is invariant under M^T and yields a contribution $(\oplus |\bullet\rangle)^N = 1$; on the other hand, if the domain of \circ survives all the way to $t = 0$, the result vanishes as it involves at least one overlap $(\circ |\bullet\rangle) = 0$. This is sketched in Fig. 2(b).

In all, we find that the average density of holes $\bar{h}_i(t)$ equals the probability that the two random walkers annihilate in t steps or less; conversely, $\bar{n}_i(t)$ equals their *survival probability*. This probability can be computed analytically, giving at large t

$$\bar{n}_i(t) = 1 - q^{-2} + ct^{-3/2} e^{-\gamma t} + \dots \quad (5)$$

for any site i in the bulk of the operator, with $c > 0$ a constant and \dots denoting subleading corrections in t [41]. The relaxation rate γ is related to the circuit’s *entanglement velocity* v_E (which sets the decay of half-system purity as $\sim q^{-v_E t}$) [43] via $\gamma = 2 \ln(q) v_E$, see [41]; the $t^{-3/2}$ is a universal correction related to the first return

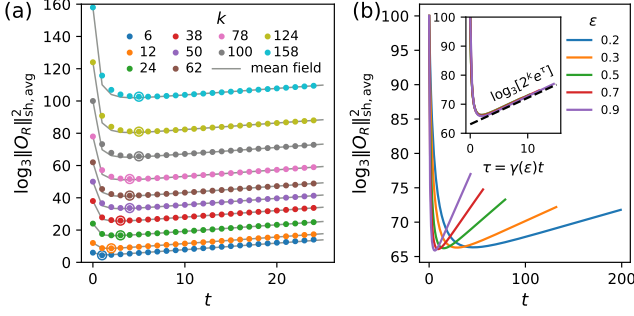


FIG. 3. (a) Shadow norm of a weight- k Pauli string O_A in an infinite 1D system of qubits ($q = 2$), under twirling by depth- t brickwork circuits of Haar-random gates (no gate dilution, $\epsilon = 1$). Data from iMPS simulations with bond dimension $\chi = 2048$. Circled dots indicate the optimal depth. (b) Same quantity for fixed $k = 100$ and variable gate dilution ϵ . Inset: same data as a function of “effective depth” $\tau = \gamma(\epsilon)t$, compared to $q^k e^{\gamma t}$ (dashed line).

of a random walker in one dimension [44]. We conjecture that the convergence to equilibrium is similarly exponential in any finite spatial dimension, and numerically verify it in two dimensions [41].

Scaling of the optimal depth. With these key results in hand, we can now return to the question of the optimal depth. By using Eq. (4) and Jensen’s inequality, we have $\|O_A\|_{\text{sh,avg}}^2 \leq (q+1)^{\bar{w}}$; in one dimension, the average weight obeys $\bar{w}(t) = \sum_i \bar{n}_i(t) \simeq \bar{\ell}(t) \bar{n}_{\text{bulk}}(t)$, with $\bar{\ell}(t) = k + 2v_B t$ the average spatial length of the twirled operator, which spreads with butterfly velocity v_B [33, 35, 45], and $\bar{n}_{\text{bulk}}(t)$ the bulk density of traceless Paulis, Eq. (5) (the structure of the operator’s fronts can be neglected at large k). The bound is minimized at depth

$$t^*(k) = \gamma^{-1} \left(\ln(k) - \frac{3}{2} \ln \ln(k) + o(\ln \ln(k)) \right) \quad (6)$$

(see [41]). At $t = t^*(k)$, the shadow norm is bounded above by $(q+1)^{(1-q^{-2})k} \times \text{poly}(k)$, exponentially smaller than the $t = 0$ (local twirling) value of $(q+1)^k$; e.g., for qubits ($q = 2$) the scaling is $3^{\frac{3}{4}k} \simeq 2.28^k$ vs 3^k . This is one of the central results of our work. The scaling $\log(k)$ (as opposed to more general $\text{polylog}(k)$ [25]) is especially important as it ensures an MPO representation for \mathcal{M}^{-1} with $\text{poly}(k)$ bond dimension, which is key to the classical computational cost of the method [25, 26].

We conjecture that $t = t^*(k)$ in fact minimizes not just the upper bound $(q+1)^{\bar{w}}$, but the shadow norm itself, and that the achievable scaling of the latter is $\text{poly}(k) \times q^k$ —nearly saturating the q^k lower bound obtained by full relaxation with no spreading. This is supported by an analytical calculation within a mean-field approximation, where we neglect correlations between occupations n_i , n_j at different sites, see [41]. We find that $\|O_A\|_{\text{sh,avg}}$ is dominated by Pauli operators of size

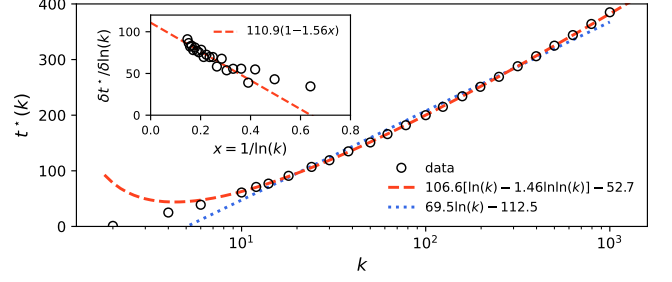


FIG. 4. Optimal depth $t^*(k)$ as a function of Pauli operator weight k , obtained from iMPS data as in Fig. 3, for k up to 1000. The gate dilution is $\epsilon = 0.05$ and bond dimension is $\chi = 2048$. Best fits to $t^*(k) = a \ln(k) + b$ (dotted line) and $t^*(k) = a[\ln(k) - c \ln \ln(k)] + b$ (dashed line) are shown. The value of the doubly-logarithmic correction is found to be $c = 1.5(2)$, consistent with the prediction in Eq. (6). Inset: discrete derivatives $\delta t^*(k)/\delta \ln(k)$, plotted vs $1/\ln(k)$, are also consistent with a doubly-logarithmic correction with $c \simeq 1.5$.

$k + 2v_B^{\text{sp}} t$, with a renormalized “saddle-point butterfly velocity” v_B^{sp} smaller than the original v_B , and equal to the entanglement velocity $v_E = \gamma/\ln(q^2)$. This, in particular, predicts the late-time behavior $\|O_A\|_{\text{sh,avg}}^2 \sim q^{k+2v_B^{\text{sp}} t} = q^k e^{\gamma t}$. Minimizing the mean-field shadow norm over t yields the same $t^*(k)$ as in Eq. (6), and thus the optimal shadow norm $\sim k q^k$.

Numerical simulations. To check the validity of the above results, we perform numerical simulations of the averaged twirling dynamics based on infinite matrix product states (iMPS) [46] (see [41] for method details).

Fig. 3(a) shows the state-averaged shadow norm for contiguous operators of various weights k in a 1D chain of qubits ($q = 2$), as a function of depth t . Three regimes are clearly visible: the $t = 0$ (local twirling) value of 3^k , a minimum at $t \sim \log(k)$, and finally exponential growth due to continued operator spreading after relaxation. In un-diluted circuits ($\epsilon = 1$) the optimal depth $t^*(k)$ takes very small integer values, severely limiting the resolution on its scaling [25]. This issue is greatly alleviated by gate dilution: as shown in Fig. 3(b), the shadow norm approximately behaves as a smooth function of an “effective depth” $\tau = \gamma(\epsilon)t$, where γ is the Pauli density relaxation rate in Eq. (5)—smaller ϵ yields a finer sampling of τ . We thus set $\epsilon = 0.05$ in order to finely resolve the scaling of $t^*(k)$, obtaining the results in Fig. 4. The data show remarkable agreement with Eq. (6), including the subleading correction $\sim \ln \ln(k)$. Note that the value of $3/2$ for the ratio of coefficients is universal (determined by the probability of first return of a random walk via Eq. (5)), which constitutes a nontrivial check of our analytical results.

Higher dimensions. While several details of the above discussion are special to one dimension, the general picture applies to systems in any finite spatial dimension. The leading-order result ($t^*(k) \sim \ln k$) depends only on the balancing of operator spreading and relaxation, based

on the notions of bulk and boundary for a geometrically contiguous subsystem. The picture changes completely in systems with all-to-all connectivity, or on expander graphs, where a subsystem’s bulk and boundary generally have comparable sizes. There the optimal twirling depth is expected to be zero, i.e., local twirling performs best. We test this expectation on a “Brownian circuit” model whose operator dynamics are described by simple, closed equations, and are amenable to exact treatment; we find the optimal depth is $t = 0$ unless the operator is supported on a sufficiently large fraction of the system ($k \gtrsim N/2$), see [41].

Discussion. We have studied how classical shadows based on shallow quantum circuits can be used to learn expectation values of Pauli operators. We have connected the sample complexity of classical shadows to the dynamics of operator weight, identifying two competing dynamical processes (operator spreading and operator relaxation) whose balance determines the optimal depth t^* of the twirling circuits. This picture elegantly explains previous numerical observations on one-dimensional systems [25, 26], and extends the result to systems in any finite dimension. Further, it shows that the optimal depth scales as $t^* = O(\ln k)$ with the weight k of the operator to be learned, as opposed to a more general $t^* = \text{polylog}(k)$ scaling [25]. This ensures the optimal protocol has a $\text{poly}(k)$ classical computational cost.

Our work opens up several directions for future research. It would be interesting to generalize our results to different settings for classical shadows, beyond shallow brickwork circuits on qudits. The recent proposals for classical shadows in analog simulators [47, 48] or on fermionic [17, 18] and bosonic [49] systems are interesting possible directions. Further, it would be interesting to extend our analysis beyond Pauli expectation values and into other properties of quantum states, such as measures of entanglement [22, 23]. The validity of our results in higher dimension also suggests interesting applications to e.g. topological or fracton codes and phases [50–55], though the classical computational complexity of shallow

shadows in higher dimension poses a nontrivial barrier.

From the mathematical point of view, our work raises two natural questions. First, is it possible to rigorously prove that depth $t^*(k)$, Eq. (6), is indeed optimal, and that the achievable shadow norm scales as $q^k \times \text{poly}(k)$? Second, is it possible to extend our results from the *state-averaged* shadow norm to the true (i.e., state-optimized) shadow norm? Doing so would provide robust guarantees on worst-case performance.

To make contact with NISQ experiments [15, 56], it would be interesting to understand the impact of noise on our results, by extending the analysis of noisy classical shadows [13, 57] to this setting.

Finally, the concept of operator relaxation, which plays a key role in our results, may be of independent interest from the point of view of quantum dynamics. While the concept of operator spreading is central to the study of quantum chaos [31–36], operator relaxation and similar diagnostics of local equilibration in operator space [34, 36, 58] are comparatively under-explored, and may prove similarly useful in understanding signatures of quantum-chaotic behavior [59].

Acknowledgments. We thank Bryan Clark, Wen Wei Ho and Hsin-Yuan Huang for discussions on classical shadows. M.I. and Y.L. are supported in part by the Gordon and Betty Moore Foundation’s EPiQS Initiative through Grant GBMF8686. T.R. and Y.L. are supported in part by the Stanford Q-FARM Bloch Postdoctoral Fellowship in Quantum Science and Engineering. V.K. acknowledges support from the US Department of Energy, Office of Science, Basic Energy Sciences, under Early Career Award Nos. DE-SC0021111, the Alfred P. Sloan Foundation through a Sloan Research Fellowship, and the Packard Foundation through a Packard Fellowship in Science and Engineering. Numerical simulations were performed on Stanford Research Computing Center’s Sherlock cluster. We acknowledge the hospitality of the Kavli Institute for Theoretical Physics at the University of California, Santa Barbara (supported by NSF Grant PHY-1748958).

-
- [1] Frank Arute, Kunal Arya, Ryan Babbush, Dave Bacon, Joseph C. Bardin, Rami Barends, *et al.*, “Quantum supremacy using a programmable superconducting processor,” *Nature* **574**, 505–510 (2019).
 - [2] Ehud Altman, Kenneth R. Brown, Giuseppe Carleo, Lincoln D. Carr, Eugene Demler, Cheng Chin, *et al.*, “Quantum Simulators: Architectures and Opportunities,” *PRX Quantum* **2**, 017003 (2021).
 - [3] Xiao Mi, Pedram Roushan, Chris Quintana, Salvatore Mandra, Jeffrey Marshall, Charles Neill, *et al.*, “Information scrambling in quantum circuits,” *Science* **374**, 1479–1483 (2021).
 - [4] Yulin Wu, Wan-Su Bao, Sirui Cao, Fusheng Chen, Ming-Cheng Chen, Xiawei Chen, *et al.*, “Strong Quantum Computational Advantage Using a Superconducting Quantum Processor,” *Physical Review Letters* **127**, 180501 (2021).
 - [5] Laird Egan, Dripto M. Debroy, Crystal Noel, Andrew Risinger, Daiwei Zhu, Debopriyo Biswas, *et al.*, “Fault-tolerant control of an error-corrected qubit,” *Nature* **598**, 281–286 (2021).
 - [6] Rajeev Acharya, Igor Aleiner, Richard Allen, Trond I. Andersen, Markus Ansmann, Frank Arute, *et al.*, “Suppressing quantum errors by scaling a surface code logical qubit,” (2022), 10.48550/arXiv.2207.06431.
 - [7] Sepehr Ebadi, Tout T. Wang, Harry Levine, Alexander Keesling, Giulia Semeghini, Ahmed Omran, *et al.*, “Quantum phases of matter on a 256-atom programmable quantum simulator,” *Nature* **595**, 227–232 (2021).
 - [8] G. Semeghini, H. Levine, A. Keesling, S. Ebadi, T. T. Wang, D. Bluvstein, *et al.*, “Probing topological spin

- liquids on a programmable quantum simulator,” *Science* **374**, 1242–1247 (2021).
- [9] Jeongwan Haah, Aram W. Harrow, Zhengfeng Ji, Xiaodi Wu, and Nengkun Yu, “Sample-Optimal Tomography of Quantum States,” *IEEE Transactions on Information Theory* **63**, 5628–5641 (2017).
 - [10] Scott Aaronson, “Shadow Tomography of Quantum States,” (2018), [10.48550/arXiv.1711.01053](#).
 - [11] Hsin-Yuan Huang, Richard Kueng, and John Preskill, “Predicting many properties of a quantum system from very few measurements,” *Nature Physics* **16**, 1050–1057 (2020).
 - [12] Marco Painsi and Amir Kalev, “An approximate description of quantum states,” (2019), [10.48550/arXiv.1910.10543](#).
 - [13] Senrui Chen, Wenjun Yu, Pei Zeng, and Steven T. Flammia, “Robust Shadow Estimation,” *PRX Quantum* **2**, 030348 (2021).
 - [14] Atithi Acharya, Siddhartha Saha, and Anirvan M. Sengupta, “Informationally complete POVM-based shadow tomography,” (2021), [10.48550/arXiv.2105.05992](#).
 - [15] G.I. Struchalin, Ya. A. Zagorovskii, E.V. Kovlakov, S.S. Straupe, and S.P. Kulik, “Experimental Estimation of Quantum State Properties from Classical Shadows,” *PRX Quantum* **2**, 010307 (2021).
 - [16] Ryan Levy, Di Luo, and Bryan K. Clark, “Classical Shadows for Quantum Process Tomography on Near-term Quantum Computers,” (2021), [10.48550/arXiv.2110.02965](#).
 - [17] Andrew Zhao, Nicholas C. Rubin, and Akimasa Miyake, “Fermionic Partial Tomography via Classical Shadows,” *Physical Review Letters* **127**, 110504 (2021).
 - [18] Kianna Wan, William J. Huggins, Joonho Lee, and Ryan Babbush, “Matchgate Shadows for Fermionic Quantum Simulation,” (2022), [10.48550/arXiv.2207.13723](#).
 - [19] Hsin-Yuan Huang, Richard Kueng, Giacomo Torlai, Victor V. Albert, and John Preskill, “Provably efficient machine learning for quantum many-body problems,” *Science* **377**, eabk3333 (2022).
 - [20] Jonathan Kunjummen, Minh C. Tran, Daniel Carney, and Jacob M. Taylor, “Shadow process tomography of quantum channels,” (2022), [10.48550/arXiv.2110.03629](#).
 - [21] Saumya Shivam, C. W. von Keyserlingk, and S. L. Sondhi, “On Classical and Hybrid Shadows of Quantum States,” (2022), [10.48550/arXiv.2206.06616](#).
 - [22] A. Elben, B. Vermersch, C. F. Roos, and P. Zoller, “Statistical correlations between locally randomized measurements: A toolbox for probing entanglement in many-body quantum states,” *Phys. Rev. A* **99**, 052323 (2019).
 - [23] Tiff Brydges, Andreas Elben, Petar Jurcevic, Benoit Vermersch, Christine Maier, Ben P. Lanyon, *et al.*, “Probing Renyi entanglement entropy via randomized measurements,” *Science* **364** (2019), [10.1126/science.aau4963](#).
 - [24] Andreas Elben, Steven T. Flammia, Hsin-Yuan Huang, Richard Kueng, John Preskill, Benoit Vermersch, *et al.*, “The randomized measurement toolbox,” (2022), [10.48550/arXiv.2203.11374](#).
 - [25] Ahmed A. Akhtar, Hong-Ye Hu, and Yi-Zhuang You, “Scalable and Flexible Classical Shadow Tomography with Tensor Networks,” (2022), [10.48550/arXiv.2209.02093](#).
 - [26] Christian Bertoni, Jonas Haferkamp, Marcel Hinsche, Marios Ioannou, Jens Eisert, and Hakop Pashayan, “Shallow shadows: Expectation estimation using low-depth random Clifford circuits,” (2022), [10.48550/arXiv.2209.12924](#).
 - [27] Mirko Arienzo, Markus Heinrich, Ingo Roth, and Martin Kliesch, “Closed-form analytic expressions for shadow estimation with brickwork circuits,” (2022), [10.48550/arXiv.2211.09835](#).
 - [28] Tom Kennedy and Hal Tasaki, “Hidden $\mathbb{Z}_2 \times \mathbb{Z}_2$ symmetry breaking in Haldane-gap antiferromagnets,” *Physical Review B* **45**, 304–307 (1992).
 - [29] Jutho Haegeman, David Perez-Garcia, Ignacio Cirac, and Norbert Schuch, “Order Parameter for Symmetry-Protected Phases in One Dimension,” *Physical Review Letters* **109**, 050402 (2012).
 - [30] Daniel Gottesman, “Stabilizer Codes and Quantum Error Correction,” (1997), [10.48550/arXiv.quant-ph/9705052](#).
 - [31] Juan Maldacena, Stephen H. Shenker, and Douglas Stanford, “A bound on chaos,” *Journal of High Energy Physics* **2016**, 106 (2016).
 - [32] Brian Swingle, Gregory Bentsen, Monika Schleier-Smith, and Patrick Hayden, “Measuring the scrambling of quantum information,” *Physical Review A* **94**, 040302 (2016).
 - [33] Adam Nahum, Sagar Vijay, and Jeongwan Haah, “Operator Spreading in Random Unitary Circuits,” *Physical Review X* **8**, 021014 (2018).
 - [34] Vedika Khemani, Ashvin Vishwanath, and David A. Huse, “Operator Spreading and the Emergence of Dissipative Hydrodynamics under Unitary Evolution with Conservation Laws,” *Phys. Rev. X* **8**, 031057 (2018).
 - [35] C. W. von Keyserlingk, Tibor Rakovszky, Frank Pollmann, and S. L. Sondhi, “Operator Hydrodynamics, OTOCs, and Entanglement Growth in Systems without Conservation Laws,” *Physical Review X* **8**, 021013 (2018).
 - [36] Tibor Rakovszky, Frank Pollmann, and C. W. von Keyserlingk, “Diffusive Hydrodynamics of Out-of-Time-Ordered Correlators with Charge Conservation,” *Phys. Rev. X* **8**, 031058 (2018).
 - [37] Wei-Ting Kuo, A. A. Akhtar, Daniel P. Arovas, and Yi-Zhuang You, “Markovian Entanglement Dynamics under Locally Scrambled Quantum Evolution,” *Physical Review B* **101**, 224202 (2020).
 - [38] Hong-Ye Hu, Soonwon Choi, and Yi-Zhuang You, “Classical Shadow Tomography with Locally Scrambled Quantum Dynamics,” (2021), [10.48550/arXiv.2107.04817](#).
 - [39] Daniel Gottesman, “The Heisenberg Representation of Quantum Computers,” (1998), [10.48550/arXiv.quant-ph/9807006](#).
 - [40] Vlad Gheorghiu, “Standard form of qudit stabilizer groups,” *Physics Letters A* **378**, 505–509 (2014).
 - [41] See Supplementary Material for the derivation of Eq. (4) and Eq. (6), results on Brownian circuits, computation of velocity scales, and additional details on the random walk mapping, mean-field approximation and numerical methods.
 - [42] We note that the shadow norm involves a maximization over ρ in order to provide worst-case guarantees. By averaging over ρ we instead consider the average performance of classical shadows across all states.
 - [43] Adam Nahum, Jonathan Ruhman, Sagar Vijay, and Jeongwan Haah, “Quantum Entanglement Growth under Random Unitary Dynamics,” *Physical Review X* **7**, 031016 (2017).
 - [44] Michael E. Fisher, “Walks, walls, wetting, and melting,” *Journal of Statistical Physics* **34**, 667–729 (1984).

- [45] Pavan Hosur, Xiao-Liang Qi, Daniel A. Roberts, and Beni Yoshida, “Chaos in quantum channels,” *Journal of High Energy Physics* **2016**, 4 (2016).
- [46] Ulrich Schollwock, “The density-matrix renormalization group in the age of matrix product states,” *Annals of Physics January 2011 Special Issue*, **326**, 96–192 (2011).
- [47] Minh C. Tran, Daniel K. Mark, Wen Wei Ho, and Soonwon Choi, “Measuring Arbitrary Physical Properties in Analog Quantum Simulation,” (2022), [10.48550/arXiv.2212.02517](#).
- [48] Max McGinley and Michele Fava, “Shadow tomography from emergent state designs in analog quantum simulators,” (2022), [10.48550/arXiv.2212.02543](#).
- [49] Simon Becker, Nilanjana Datta, Ludovico Lami, and Cambyse Rouze, “Classical shadow tomography for continuous variables quantum systems,” (2022), [10.48550/arXiv.2211.07578](#).
- [50] A. Yu. Kitaev, “Fault-tolerant quantum computation by anyons,” *Annals of Physics* **303**, 2–30 (2003).
- [51] Jeongwan Haah, “Local stabilizer codes in three dimensions without string logical operators,” *Physical Review A* **83**, 042330 (2011).
- [52] Rahul M. Nandkishore and Michael Hermele, “Fractons,” *Annual Review of Condensed Matter Physics* **10**, 295–313 (2019).
- [53] Michael Pretko, Xie Chen, and Yizhi You, “Fracton phases of matter,” *International Journal of Modern Physics A* **35**, 2030003 (2020).
- [54] Arpit Dua, Isaac H. Kim, Meng Cheng, and Dominic J. Williamson, “Sorting topological stabilizer models in three dimensions,” *Physical Review B* **100**, 155137 (2019).
- [55] Arpit Dua, Aleksander Kubica, Liang Jiang, Steven T. Flammia, and Michael J. Gullans, “Clifford-deformed Surface Codes,” (2022), [10.48550/arXiv.2201.07802](#).
- [56] “Quantum Computing in the NISQ era and beyond,” **2**, [10.22331/q-2018-08-06-79](#).
- [57] Dax Enshan Koh and Sabee Grewal, “Classical Shadows With Noise,” *Quantum* **6**, 776 (2022).
- [58] Sivaprasad Omanakuttan, Karthik Chinni, Philip Daniel Blocher, and Pablo M. Poggi, “Scrambling and quantum chaos indicators from long-time properties of operator distributions,” (2022), [10.48550/arXiv.2211.15872](#).
- [59] Hrant Gharibyan, Masanori Hanada, Stephen H. Shenker, and Masaki Tezuka, “Onset of random matrix behavior in scrambling systems,” *Journal of High Energy Physics* **2018**, 124 (2018).
- [60] Nima Lashkari, Douglas Stanford, Matthew Hastings, Tobias Osborne, and Patrick Hayden, “Towards the fast scrambling conjecture,” *Journal of High Energy Physics* **2013**, 22 (2013).
- [61] Tianci Zhou and Xiao Chen, “Operator dynamics in a Brownian quantum circuit,” *Phys. Rev. E* **99**, 052212 (2019).
- [62] Lorenzo Piroli, Christoph Sunderhauf, and Xiao-Liang Qi, “A Random Unitary Circuit Model for Black Hole Evaporation,” *Journal of High Energy Physics* **2020**, 63 (2020).

Supplemental Material: Operator relaxation and the optimal depth of classical shadows

Matteo Ippoliti, Yaodong Li, Tibor Rakovszky, and Vedika Khemani
Department of Physics, Stanford University, Stanford, CA 94305

CONTENTS

S1. Derivation of shadow norm formula	1
A. Computation of the eigenvalues of \mathcal{M}	1
B. State-averaged shadow norm	2
C. Local and global twirling	2
S2. Random walk picture for operator relaxation	3
A. Update rules and mapping to random walk	3
B. Survival probability	3
C. Higher dimension	4
S3. Minimization of the upper bound	4
S4. Mean-field approximation to the shadow norm	5
A. Saddle-point bulk density	5
B. Mean-field result	6
C. Optimal depth	7
S5. Computation of velocity scales with gate dilution	7
S6. Details on iMPS numerical simulations	9
S7. Results on Brownian circuit	10

S1. DERIVATION OF SHADOW NORM FORMULA

Here we provide technical details involved in the derivation of our main result on the shadow norm of Pauli operators, Eq. (4).

A. Computation of the eigenvalues of \mathcal{M}

Using the fact that Pauli operators are eigenmodes of \mathcal{M} [25, 26], $\mathcal{M}(O_A) = \lambda_A O_A$, and the expression for the measurement channel with locally-scrambled twirling ensemble

$$\mathcal{M}[O_A] = D \int dU U^\dagger |0\rangle\langle 0| U \langle 0| U O_A U^\dagger |0\rangle, \quad (\text{S1})$$

(where we used the locally-scrambled property to replace each bitstring state $|b\rangle$ with $|0\rangle$, hence the factor of Hilbert space dimension D). we can compute the eigenvalues λ_A via

$$\lambda_A = \frac{1}{D} \text{Tr}(O_A \mathcal{M}[O_A]) = \int dU \langle 0| U O_A U^\dagger |0\rangle^2. \quad (\text{S2})$$

Next, we write $U O_A U^\dagger \equiv O_A(t)$, and expand it in the Pauli basis: $O_A(t) = \sum_P \alpha_P(t) P$, where P ranges over the whole N -qudit Pauli group and $\alpha_P(t) = \text{Tr}(P O_A(t))/D$. Furthermore, we exploit the locally-scrambled property of the twirling ensemble to replace $|0\rangle$ with a Haar-random product state, $|\Psi\rangle = \bigotimes_{i=1}^N |\psi_i\rangle$, with each $|\psi_i\rangle$ an independent Haar-random state of a q -state qudit. We obtain

$$\lambda_A = \int dU \int d\Psi \langle \Psi | \left(\sum_P \alpha_P(t) P \right) | \Psi \rangle^2 = \sum_{P, P'} \int dU \alpha_P(t) \alpha_{P'}(t) \int d\Psi \langle \Psi | P | \Psi \rangle \langle \Psi | P' | \Psi \rangle \quad (\text{S3})$$

Owing to random dephasing, the sum is restricted to $P = P'$: if e.g. $P|_i = X$ and $P'|_i = Z$, then a Clifford rotation Z_i changes the sign of P but not P' , while leaving the $d\Psi$ measure invariant; thus the integral must vanish. The same reasoning applies whenever P and P' differ on any site. Thus

$$\lambda_A = \sum_P \overline{|\alpha_P(t)|^2} \int d\Psi \langle \Psi | P | \Psi \rangle^2 = \sum_P \overline{|\alpha_P(t)|^2} (q+1)^{-|P|}, \quad (\text{S4})$$

where $|P|$ denotes the Hamming weight of P , i.e. the number of non-identity Pauli matrices in P , and $\overline{[\cdots]} \equiv \int dU [\cdots]$. The result follows from the single-qudit Haar integral

$$\int d\psi_i \langle \psi_i | O_i | \psi_i \rangle^2 = \begin{cases} 1/(q+1) & \text{if } O_i \text{ is a traceless Pauli matrix,} \\ 1 & \text{if } O_i \text{ is the identity.} \end{cases} \quad (\text{S5})$$

Finally, by collecting all Pauli strings of the same Hamming weight in the sum, we arrive at the result:

$$\lambda_A = \sum_w (q+1)^{-w} \sum_{P:|P|=w} \overline{|\alpha_P(t)|^2} = \sum_w (q+1)^{-w} \pi_{A,t}(w), \quad (\text{S6})$$

where the last equality defines the weight distribution $\pi_{A,t}(w)$.

B. State-averaged shadow norm

Here we derive the identity $\|O_A\|_{\text{sh,avg}}^2 = \lambda_A^{-1}$. Note that this was already observed in Refs. [25, 26]; we include a derivation here for the sake of clarity and completeness.

The variance of the estimator \hat{o} is comprised of two terms: $\mathbb{E}(\hat{o}^2)$ and $(\mathbb{E}\hat{o})^2$. The latter is equal to $\langle O_A \rangle^2$ and thus of order 1 for a Pauli operator. We focus on the former:

$$\mathbb{E}_{U,b}(\hat{o}^2) = \int dU \sum_b \langle b | U \rho U^\dagger | b \rangle \text{Tr}[O_A \mathcal{M}^{-1}(U^\dagger | b \rangle \langle b | U)]^2. \quad (\text{S7})$$

By using the fact that \mathcal{M}^{-1} is self-adjoint (evident from the fact that it has an orthonormal eigenbasis with real eigenvalues), and that $\mathcal{M}^{-1}(O_A) = \lambda_A^{-1} O_A$, we arrive at

$$\mathbb{E}_{U,b}(\hat{o}^2) = \lambda_A^{-2} D \int dU \langle 0 | U \rho U^\dagger | 0 \rangle \langle 0 | U O_A U^\dagger | 0 \rangle^2, \quad (\text{S8})$$

where we again used that the ensemble of unitaries is locally scrambled. We now take an average over states, replacing $\rho \mapsto I/D$ (as the expression is linear in ρ , the average can be taken over any state 1-design, e.g. the computational basis), and obtain

$$\mathbb{E}_\rho \mathbb{E}_{U,b}(\hat{o}^2) = \lambda_A^{-2} \int dU \langle 0 | U O_A U^\dagger | 0 \rangle^2 = \lambda_A^{-1} \quad (\text{S9})$$

where the last equality follows from recognizing the expression in Eq. (S2) for λ_A .

C. Local and global twirling

Here we show how to recover the well-known results for local and global twirling [11] from Eq. (4). The local twirling case is recovered for $t = 0$ (note t measures the number of two-qudit gates in the circuit, but initial and final layers of random one-qudit Clifford gates is always assumed). We have $\pi_{A,0}(w) = \delta_{w,k}$ (single-qudit gates cannot change the weight of a Pauli operator), thus

$$\|O_A\|_{\text{sh,avg}}^2 = \left[\sum_w \pi_{A,0}(w) (q+1)^{-w} \right]^{-1} = (q+1)^k, \quad (\text{S10})$$

recovering the well-known 3^k result for qubits ($q = 2$). Global twirling is recovered for $t \rightarrow \infty$. In this limit $O_A(t)$ becomes a random (traceless) Pauli operator. Then, the weight distribution approximately factors across different

sites, with each site hosting a random Pauli matrix (the only correlation comes from removing the global identity operator; this can be neglected for large N). As there are q^2 Pauli matrices (including the identity), we have an “empty” site (i.e. an identity) with probability q^{-2} and an “occupied” site (i.e. a traceless Pauli) otherwise. Thus we have

$$\|O\|_{\text{sh,avg}}^{-2} = \prod_i \sum_{n_i=0,1} (q+1)^{-n_i} \text{Prob}(n_i) = \prod_i \left(q^{-2} + \frac{1-q^{-2}}{q+1} \right) = q^{-N} = \|O\|_F^{-2}, \quad (\text{S11})$$

i.e. the shadow norm equals the Frobenius norm, as expected for global twirling.

S2. RANDOM WALK PICTURE FOR OPERATOR RELAXATION

Here we present a detailed discussion of the mapping of operator relaxation to a random-walk problem.

A. Update rules and mapping to random walk

We aim to describe the evolution of the vector $p_{\mathbf{n}}$ of probabilities of occupation configurations $\mathbf{n} \in \{0,1\}^N$, where n_i represents the occupation of site i in the (identity, traceless Pauli) basis.

The identity on two qudits is invariant under any unitary, thus $|\circ\circ\rangle \mapsto |\circ\circ\rangle$; under Haar-random two-qudit gates, any traceless Pauli operator maps onto one of the $q^4 - 1$ traceless Pauli operators with equal probability, thus $|\circ\bullet\rangle \mapsto a|\circ\bullet\rangle + a|\bullet\circ\rangle + (1-2a)|\bullet\bullet\rangle$, etc, where $a = 1/(q^2 + 1)$ (the fraction of single-qudit traceless Paulis out of all two-qudit traceless Paulis, $(q^2 - 1)/(q^4 - 1)$). It follows that the two-site update matrix in the $\{|\circ\circ\rangle, |\circ\bullet\rangle, |\bullet\circ\rangle, |\bullet\bullet\rangle\}$ basis reads

$$M_{\text{Haar}} = \begin{pmatrix} 1 & 0 & 0 & 0 \\ 0 & a & a & a \\ 0 & a & a & a \\ 0 & 1-2a & 1-2a & 1-2a \end{pmatrix} \quad (\text{S12})$$

Introducing the vector $|\oplus\rangle = |\circ\rangle + |\bullet\rangle$, from the fact that M_{Haar} is a stochastic matrix (i.e. columns add up to unity) we immediately have $M_{\text{Haar}}^T |\oplus\oplus\rangle = |\oplus\oplus\rangle$, thus a domain of \oplus states is an eigenstate of the backwards dynamics. Furthermore, we have by explicit calculation that $M_{\text{Haar}}^T |\oplus\oplus\rangle = (1-a)|\circ\circ\rangle + a|\oplus\oplus\rangle$. This implies that, under the backward evolution, domains of \circ and \oplus states are preserved, and the location of the domain wall hops by one site either left or right, with probabilities $a, 1-a$ that favor the growth of the \circ domain (as $a = 1/(q^2 + 1) < 1/2$).

In the presence of gate dilution, we have $M(\epsilon) = (1-\epsilon)I + \epsilon M_{\text{Haar}}$, and thus the update rule for a domain wall between \oplus and \circ :

$$|\overbrace{\oplus \cdots \oplus}^x \overbrace{\circ \cdots \circ}^{N-x}\rangle \mapsto \epsilon a |\overbrace{\oplus \cdots \oplus}^{x+1} \overbrace{\circ \cdots \circ}^{N-x-1}\rangle + (1-\epsilon) |\overbrace{\oplus \cdots \oplus}^x \overbrace{\circ \cdots \circ}^{N-x}\rangle + \epsilon(1-a) |\overbrace{\oplus \cdots \oplus}^{x-1} \overbrace{\circ \cdots \circ}^{N-x+1}\rangle. \quad (\text{S13})$$

This update is illustrated in Fig. 2(a) in the main text.

B. Survival probability

For the purpose of computing the average density of holes $\overline{h_i}(t)$, the final boundary condition (Fig.2(a) in the main text) is $|\cdots \oplus \oplus \oplus \circ \oplus \oplus \cdots\rangle$, where \circ is at site i and the 1D chain is infinite (though in practice length t on both sides suffices, due to the unitary light cone). This corresponds to two random walkers being initialized at positions $x_1 = i, x_2 = i + 1$ (bond i being to the left of site i).

Let us focus on $\epsilon = 0$ (un-diluted circuit). The relative coordinate $x_r \equiv x_2 - x_1$ takes exactly two steps per unit time (as each of the two walkers $x_{1,2}$ takes one step), with $\text{Prob}(\delta x = +1) = 1-a$ and $\text{Prob}(\delta x = -1) = a$. The walker is annihilated if it reaches $x_r = 0$ in t steps or less, it survives otherwise. If it survives, then the contribution to $\overline{h_i}(t)$ includes overlaps $\langle \circ | \bullet \rangle = 0$, and thus vanishes (see Fig. 2(b) in the main text). Thus $\overline{h_i}(t)$ equals the probability of annihilation at or before time t .

The probability of annihilation at time τ , i.e. in $2\tau + 1$ steps (note that at $t = 0$ only one out of $x_{1,2}$ takes a step) is given by

$$P(\text{annihilation at time } \tau) = a^{\tau+1}(1-a)^\tau C_\tau \simeq \frac{a[4a(1-a)]^\tau}{\sqrt{\pi\tau^3}} \quad (\text{S14})$$

where $C_\tau = \frac{1}{\tau+1} \binom{2\tau}{\tau}$ are the Catalan numbers, whose large- τ expansion is $C_\tau \simeq 4^\tau / \sqrt{\pi\tau^3}$. Defining

$$e^{-\gamma} \equiv 4a(1-a) = \left(\frac{2q}{q^2+1} \right)^2 \quad (\text{S15})$$

(note $\gamma > 0$) and integrating over $\tau \leq t$, we see that at large t ,

$$P(\text{annihilation at time} \leq t) = \text{const.} - \frac{a}{\gamma\sqrt{\pi}} t^{-3/2} e^{-\gamma t} \quad (\text{S16})$$

up to subleading corrections. We can determine the integration constant as follows: by reversing the bias ($a \mapsto 1-a$), the walker should annihilate with unit probability as $t \rightarrow \infty$; this implies $\sum_\tau a^\tau (1-a)^{\tau+1} C_\tau = 1$; exploiting this identity, we have that the late-time asymptotic value of the annihilation probability is $\sum_\tau a^{\tau+1} (1-a)^\tau C_\tau = \frac{a}{1-a} = \frac{1}{q^2}$. This is in agreement with the expected density of identity operators \bar{h}_i at late times. With this, we conclude that

$$\bar{n}_i(t) = P(\text{survival up to } t) \simeq 1 - \frac{1}{q^2} + \frac{1}{\sqrt{\pi}\gamma(q^2+1)} t^{-3/2} e^{-\gamma t} \quad (\text{S17})$$

at large t , up to subleading corrections.

The functional form $t^{-3/2} e^{-\gamma t}$ is a universal property of a biased random walk's first return time, and thus holds with gate dilution as well, though the value of γ and the multiplicative constant will change.

C. Higher dimension

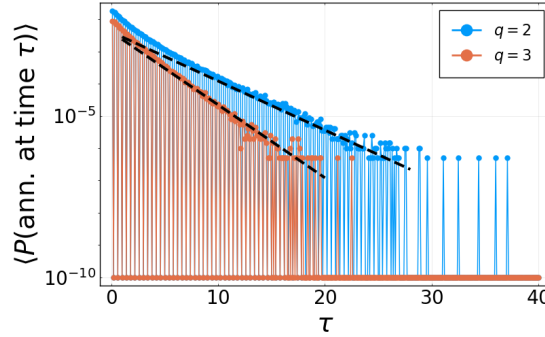


FIG. S1. Numerical results for the probability of annihilation of the \bigcirc domain at time τ , for qudits with $q = 2$ and 3 in two spatial dimensions. Data from Monte Carlo simulation of the Markov process in the \bigcirc, \oplus basis, without gate dilution ($\epsilon = 1$). Dashed lines are exponential fits.

Although the random walk picture only strictly works in one dimension, the Markov process in Eq. (S12) is defined for any circuit with 2-local gates, and in particular can be used to compute the mean operator density in higher dimensions. Here we simulate this process in two dimensions, with the state $|\bigcirc\rangle$ on a single site, and the state $|\oplus\rangle$ on all remaining sites. The boundary between the two domains, when present, moves under Eq. (S13). We plot $P(\text{annihilation at time } \tau)$ in Fig. S1. The result is similar to the one dimensional case, Eq. (S14), namely to leading order

$$P(\text{annihilation at time } \tau) \propto e^{-\gamma(q)\tau}. \quad (\text{S18})$$

We expect this result to hold in general in any finite dimension. As a consequence, the leading-order result $t^* \propto \ln k$ should hold in all finite dimensions, with possibly different subleading corrections.

S3. MINIMIZATION OF THE UPPER BOUND

Here we show details on the minimization of the upper bound to the shadow norm, $\|O_A\|_{\text{sh,avg}}^2 \leq (q+1)^{\bar{w}}$. We aim to find the minimum over t of the average weight $\bar{w}(t)$, which controls the upper bound $\|O_A\|_{\text{sh,avg}}^2 \leq (q+1)^{\bar{w}}$.

The average spatial length of the twirled Pauli operator $O_A(t)$ is $\bar{\ell}(t) = k + 2v_B t$, where v_B is the average butterfly velocity of the unitary circuit U . Neglecting the front structure of the operator (i.e. dependence of the density \bar{n}_i on position i inside the support of the operator), we have $\bar{w} \simeq \bar{\ell}(t)\bar{n}_i(t)$, where $\bar{n}_i(t) = 1 - 1/q^2 + cf(t)$ for $c > 0$ constant and $f(t) = t^{-3/2}e^{-\gamma t}$. Minimization of \bar{w} in this approximation gives

$$2v_B [1 - 1/q^2 + cf(t)] = -(k + 2v_B t)cf'(t). \quad (\text{S19})$$

We are interested in the asymptotics for large Pauli operators and late times ($k, t \gg 1$), thus we may drop $cf(t)$ in the l.h.s. (as it is $\ll 1$), and in the r.h.s. we may simplify $f'(t) = -[\gamma + \frac{3}{2t}]f(t) \simeq -\gamma f(t)$; thus

$$2v_B(1 - 1/q^2) \simeq \gamma c(k + 2v_B t)t^{-3/2}e^{-\gamma t}. \quad (\text{S20})$$

It follows (since the l.h.s. is finite) that the minimum is achieved for $t \sim \log(k)$; thus $k \gg t \gg 1$. Dropping $2v_B t$ in the r.h.s., we get

$$t^{3/2}e^{\gamma t} \simeq \frac{\gamma}{2v_B(1 - 1/q^2)}k. \quad (\text{S21})$$

Taking the logarithm, we arrive at the recursive equation

$$t^* = \frac{1}{\gamma} \left(\ln(k) - \frac{3}{2} \ln(t^*) \right) + \text{const.} \quad (\text{S22})$$

Iterating the recursion once (i.e. setting $t^* \mapsto \frac{1}{\gamma} \ln(k) + \dots$ in the r.h.s.) yields the result in the main text, Eq. (6).

At depth $t^*(k)$, the upper bound reads

$$\|O_A\|_{\text{sh,avg}}^2 \leq (q+1)^{(k+O(\log(k)))(1-q^{-2}+O(1/k))} = (q+1)^{(1-q^{-2})k} \times \text{poly}(k). \quad (\text{S23})$$

S4. MEAN-FIELD APPROXIMATION TO THE SHADOW NORM

Here we present details about the analytical mean-field approximation to the shadow norm. The key idea is to drop correlations between Pauli densities at different sites, taking the n_i to be independently, identically distributed (i.i.d.) binomial random variables, in order to factor the average $\overline{(q+1)^{-w}}$ into a product of on-site averages. However, there is an important subtlety in how to treat the size of the operator's support, as explained below.

A. Saddle-point bulk density

While we have computed the *average* bulk density of Paulis inside a long operator $\bar{n}_i(t)$, Eq. (5), the dominant contribution to the shadow norm comes from Pauli strings at below-equilibrium density. This is due to the exponential suppression induced by the $(q+1)^{-w}$ factor. Let us consider a Pauli operator on N sites, with $\bar{n}_i(t) \equiv 1 - q^{-2} + cf(t)$ for all sites i ; within a mean-field approximation, treating each n_i as an i.i.d. binomial distribution with $\text{Prob}(n_i = +1) = \bar{n}_i(t)$, we have

$$\overline{(q+1)^{-w}} = \sum_{w=1}^N \binom{N}{w} (1 - q^{-2} + cf(t))^w (q^{-2} - cf(t))^{N-w} (q+1)^{-w} = \left(\frac{1}{q} - \frac{q}{q+1} cf(t) \right)^N. \quad (\text{S24})$$

We define a “saddle point” density n_{sp} by setting the above equal to $(q+1)^{-Nn_{\text{sp}}}$ (in other words, n_{sp} is defined so that if the weight distribution were a δ -function centered at $w = Nn_{\text{sp}}$, we would recover the correct answer for $\overline{(q+1)^{-w}}$). This gives

$$n_{\text{sp}} = \frac{\ln(q)}{\ln(q+1)} - \frac{\ln(1 - q^2 cf(t)/(q+1))}{\ln(q+1)} \simeq \frac{\ln(q)}{\ln(q+1)} + \frac{q^2 cf(t)}{(q+1) \ln(q+1)} \quad (\text{S25})$$

where we linearized in $f(t) \ll 1$ in the second step. Note that $n_{\text{sp}} < \bar{n}$; in particular for large q we have $n_{\text{sp}} \simeq 1 - 1/q$ vs $\bar{n} = 1 - 1/q^2$.

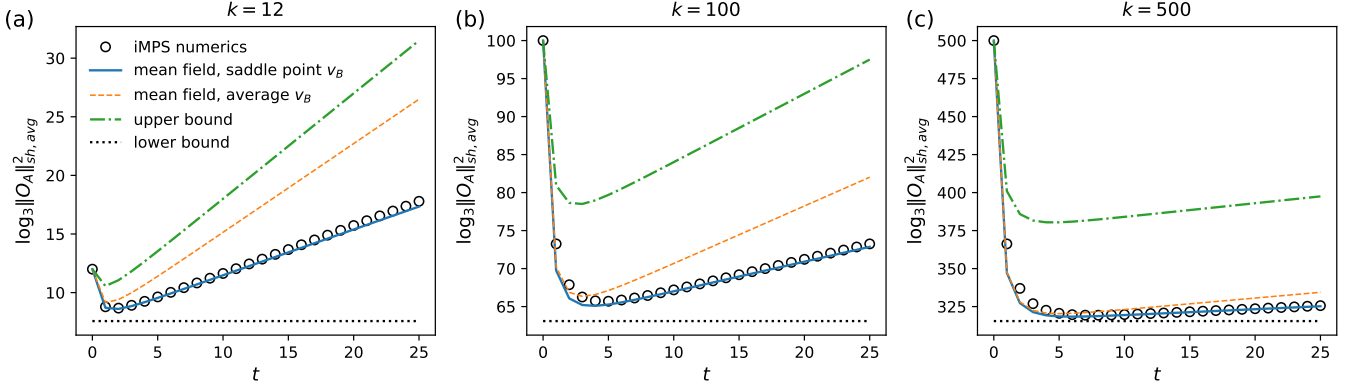


FIG. S2. Comparing the mean-field result for $\|O_A\|_{\text{sh,avg}}^2$, Eq. (S30) (solid line), to iMPS numerical data (circles), the upper bound $\|O_A\|_{\text{sh,avg}}^2 \leq (q+1)^{\overline{w}}$ (dot-dashed line), the lower bound $\|O_A\|_{\text{sh,avg}}^2 \geq q^k$ (dotted line), and an alternative mean-field approximation where the average butterfly velocity v_B is used instead of the saddle-point value v_B^{sp} (dashed line).

B. Mean-field result

Let us now consider the biased random walk of an operator's front, x . This moves outward with probability $1-a$ and inward otherwise, giving a butterfly velocity $v_B = 1-2a$ for the *average* position of the front. Let us consider the left and right endpoints of the operator, x_1 and x_2 , each describing a random walk as above (with average velocity $\pm v_B$). Assuming that all sites between the two fronts host an i.i.d. local density n_i with mean $\overline{n_i}$, we find that the contribution of such an operator to the (inverse squared) shadow norm $\|O_A\|_{\text{sh,avg}}^{-2}$ is $(q+1)^{n_{\text{sp}}(x_1-x_2)}$, by the definition of n_{sp} given above. As long as $k \gg t$, the two endpoints cannot meet and we may treat the random walks as independent; thus

$$\|O_A\|_{\text{sh,avg}}^{-2} \simeq \sum_{x_1, x_2} \text{Prob}(x_1) \text{Prob}(x_2) (q+1)^{-n_{\text{sp}}(x_2-x_1)} = (q+1)^{-n_{\text{sp}}k} \left(\sum_{x=-t}^t \text{Prob}(x) (q+1)^{-n_{\text{sp}}x} \right)^2 \quad (\text{S26})$$

where x describes the outward displacement of either endpoint from its initial location. The sum in parenthesis yields

$$\sum_{x=-t}^{+t} \binom{t}{\frac{t+x}{2}} a^{\frac{t-x}{2}} (1-a)^{\frac{t+x}{2}} (q+1)^{-n_{\text{sp}}x} = (a(q+1)^{n_{\text{sp}}} + (1-a)(q+1)^{-n_{\text{sp}}})^t \quad (\text{S27})$$

Setting this equal to $q^{-v_B^{\text{sp}}t}$ defines the “saddle point butterfly velocity”

$$v_B^{\text{sp}} = \frac{\ln(ag + (1-a)/g)}{\ln q}, \quad g = (q+1)^{n_{\text{sp}}} = q \left(1 - \frac{q^2 c f(t)}{q+1} \right)^{-1} \quad (\text{S28})$$

We note that at equilibrium, i.e. for $t \rightarrow \infty$ ($f(t) \rightarrow 0$), this gives

$$v_B^{\text{sp}} = \log_q \frac{q^2 + 1}{2q}, \quad (\text{S29})$$

equal to the entanglement velocity v_E [43] and proportional to the Pauli density relaxation rate $\gamma = 2 \ln \frac{q^2+1}{2q}$, Eq. (S15); namely we have $q^{2v_B^{\text{sp}}} = e^\gamma$.

With this notation, we may rewrite Eq. (S27) to obtain an explicit mean-field approximation to the shadow norm,

$$\|O_A\|_{\text{sh,avg}}^2 \simeq (q+1)^{n_{\text{sp}}k} q^{2v_B^{\text{sp}}t} = \left(\frac{1}{q} - \frac{q c f(t)}{q+1} \right)^{-k} q^{2v_B^{\text{sp}}t}. \quad (\text{S30})$$

Notably, at late times this predicts

$$\|O_A\|_{\text{sh,avg}}^2 \simeq q^{k+2v_B^{\text{sp}}t} \simeq q^k e^{\gamma t}, \quad (\text{S31})$$

where we used the fact that $v_B^{\text{sp}} \rightarrow \gamma/2 \ln(q)$ at late times, Eq. (S29). This is found to be in quantitative agreement with numerical data, see Fig. S2.

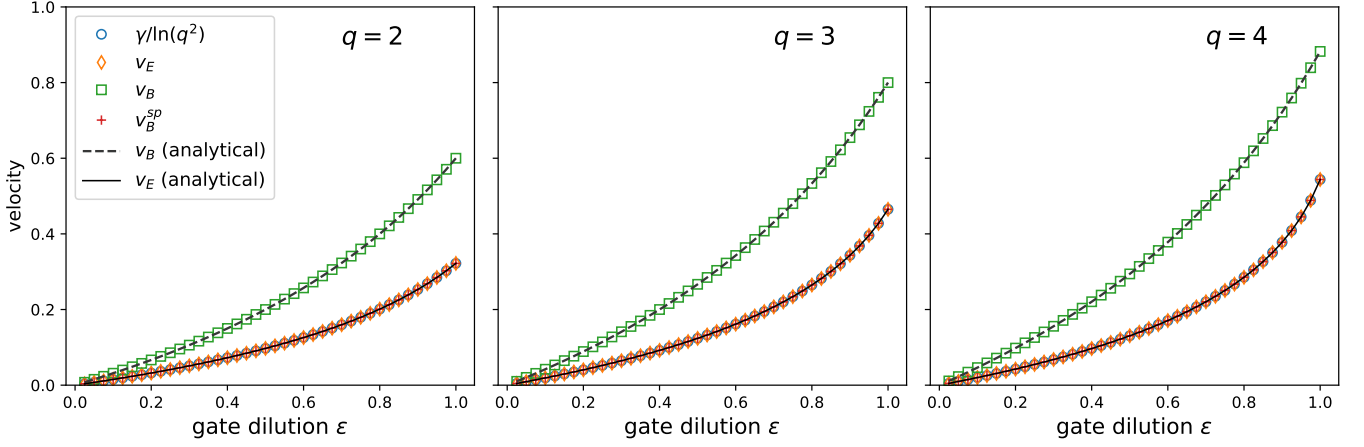


FIG. S3. Velocity scales γ (Pauli density relaxation rate), v_E (entanglement velocity), v_B (butterfly velocity), and v_B^{sp} (saddle-point butterfly velocity) computed numerically as a function of gate dilution ϵ , for qudit dimension $q = 2$ (left), 3 (center), 4 (right). v_B and v_E agree with their respective analytical predictions, Eq. (S35) and Eq. (S38). Furthermore, we find that within numerical error, $v_E = v_B^{\text{sp}} = \gamma / \ln(q^2)$ across all values of ϵ and q , as predicted.

C. Optimal depth

Finally we minimize Eq. (S30) to obtain the mean-field prediction for the optimal depth:

$$[2v_B^{\text{sp}} + 2t\partial_t v_B^{\text{sp}}] \ln\left(\frac{1}{q} - \frac{qc f(t)}{q+1}\right) - (k + 2v_B^{\text{sp}}t) \frac{qc f'(t)}{1 + q^{-1} - qc f(t)} = 0 \quad (\text{S32})$$

Discarding small terms for $k \gg t \gg 1$ we arrive at

$$k f(t) = \frac{2v_B^{\text{sp}}(1 + 1/q) \ln(q)}{\gamma qc} \quad (\text{S33})$$

which upon taking the logarithm of both sides yields Eq. (S22), and thus the same optimal depth $t^*(k) = \frac{1}{\gamma}(\ln(k) - (3/2)\ln\ln(k) + \dots)$. The mean-field shadow norm at $t^*(k)$ is $q^k \times \text{poly}(k)$.

S5. COMPUTATION OF VELOCITY SCALES WITH GATE DILUTION

Here we show numerical and analytical results for the various velocity scales in the problem in the presence of gate dilution, $0 \leq \epsilon < 1$. The relevant scales are: γ , “relaxation rate” of the Pauli density; v_B , butterfly velocity, governing operator spreading on average; v_B^{sp} , governing operator spreading at the saddle point in the shadow norm calculation; and v_E , entanglement velocity, characterizing entanglement growth. Their values in un-diluted Haar-random brickwork circuits ($\epsilon = 1$) are easily computed analytically. We have $v_B = \frac{q^2-1}{q^2+1}$, $v_E = v_B^{\text{sp}} = \log_q \frac{q^2+1}{2q}$ (see Eq. (S29)), and $\gamma = 2 \ln \frac{q^2+1}{2q} = 2 \ln(q) v_E$.

The corresponding values for $0 < \epsilon \leq 1$ and several local Hilbert space dimensions q are shown in Fig. S3. The methods used for the computation are described below for each quantity. Remarkably, we find that the equality $v_E = v_B^{\text{sp}} = \gamma / \ln(q^2)$, initially derived at $\epsilon = 1$, persists to $\epsilon < 1$, suggesting that this might hold more generally (i.e. beyond diluted Haar-random brickwork circuits).

Butterfly velocity. v_B is the average velocity of the random walk described by the right endpoint of a Pauli operator, i.e. the rightmost site x hosting a traceless Pauli matrix (of course the left endpoint has average velocity $-v_B$). The transition probabilities for x depend on the parity of $x + t$, due to the brickwork structure of the circuit. We have

$$\text{if } x + t \text{ is even: } \begin{cases} \text{Prob}(\delta x = +1) = \epsilon(1 - a) \\ \text{Prob}(\delta x = 0) = 1 - \epsilon + \epsilon a \end{cases}, \quad \text{if } x + t \text{ is odd: } \begin{cases} \text{Prob}(\delta x = 0) = 1 - \epsilon a \\ \text{Prob}(\delta x = -1) = \epsilon a \end{cases} \quad (\text{S34})$$

From these transition rules we find that the steady-state probability of $x + t$ being even is $\text{Prob}(x + t \text{ even}) = (1 - \epsilon a)/(2 - \epsilon)$, and thus

$$\begin{aligned} v_B(\epsilon) &= \overline{\delta x} = \text{Prob}(x + t \text{ even})\text{Prob}(\delta x = +1|x + t \text{ even}) - \text{Prob}(x + t \text{ odd})\text{Prob}(\delta x = -1|x + t \text{ odd}) \\ &= \frac{\epsilon}{2 - \epsilon}(1 - 2a) = \frac{\epsilon}{2 - \epsilon}v_B(1). \end{aligned} \quad (\text{S35})$$

entanglement velocity. We use the recursion relation for the purity from Ref. [43], adapted to the case with gate dilution: if $\mathcal{P}(x, t)$ is the subsystem purity for a cut at bond x at time t , we have

$$\mathcal{P}(x, t) = \begin{cases} (1 - \epsilon)\mathcal{P}(x, t - 1) + \epsilon \frac{q}{q^2 + 1} [\mathcal{P}(x - 1, t - 1) + \mathcal{P}(x + 1, t - 1)] & \text{if } x + t \text{ is even,} \\ \mathcal{P}(x, t - 1) & \text{if } x + t \text{ is odd.} \end{cases} \quad (\text{S36})$$

Assuming $\mathcal{P}(x, t) \sim q^{-v_E t}$, we obtain a quadratic equation for q^{v_E} :

$$1 = (1 - \epsilon)q^{2v_E} + \epsilon \frac{2q}{q^2 + 1} q^{v_E} \quad (\text{S37})$$

which can be solved to obtain

$$v_E(\epsilon) = \log_q \left[\frac{\epsilon}{2(1 - \epsilon)} \frac{2q}{q^2 + 1} \left(\sqrt{1 + \frac{1 - \epsilon}{\epsilon^2} \left(\frac{q^2 + 1}{q} \right)^2} - 1 \right) \right]. \quad (\text{S38})$$

We note that the recursion for $\mathcal{P}(x, t)$ can be thought of as a random walk with steps

$$\begin{cases} (x, t) \mapsto (x + 1, t - 1) [\text{prob. } p_+ = \epsilon q / (q^2 + 1)] \\ (x, t) \mapsto (x + 1, t - 2) [\text{prob. } p_0 = 1 - \epsilon] \\ (x, t) \mapsto (x - 1, t - 1) [\text{prob. } p_- = \epsilon q / (q^2 + 1)] \end{cases} \quad (\text{S39})$$

where the “probabilities” p_{\pm}, p_0 are not normalized: $p_+ + p_0 + p_- < 1$. The purity at time t is given by the total survival probability. This point of view will be useful for connecting v_E to γ later.

Saddle-point butterfly velocity. We simulate the random walk for the Pauli endpoint, Eq. (S34), starting from an initial probability distribution $p_0(x) = \delta_{x, x_0}$ and obtain a late-time distribution $p_t(x)$. Then we fit $q^{-x(t)} = \sum_x p_t(x) q^{-x}$ to $q^{-v_B^{\text{sp}} t}$, following the discussion in Sec. S4.

We note that this calculation is formally identical to the one used for computing the entanglement velocity v_E from an operator-spreading picture in Ref. [35] (in particular see Eq. (24) therein). There, the purity of a subsystem A is computed by analyzing the propagation of operator endpoints across the subsystem boundary; an exponential weighting factor q^{-x} arises from the counting of (diagonal) Pauli operators whose endpoint is initially a distance x from the entanglement cut, giving rise to the same sum. It follows that $v_B^{\text{sp}} = v_E$.

Pauli density relaxation rate. As explained in Sec. S2, the relaxation of $\overline{n_i}(t)$ is determined by the annihilation probability of two biased random walkers $x_1 \leq x_2$ (representing the boundaries of a domain of \bigcirc in a background of \oplus states). Without dilution it is straightforward to derive $\gamma = 2 \ln \frac{q^2 + 1}{2q}$ (equal to $2 \ln(q) v_E$) by considering the random walk of the relative coordinate. The $\epsilon < 1$ case can be analyzed in a similar way. Each walker $x_{1,2}$ lives on a bond on a 1D lattice, and can hop only when a gate acts on that bond. It is helpful to consider a 2D square lattice in space-time with sites corresponding to gates in the brickwork circuit, i.e. (x, t) with $x + t$ even, Fig. S4(a). The walkers start from $(x_1, t) = (0, 1)$ and $(x_2, t) = (1, 0)$ and can hop as follows:

$$(x_1, t) \mapsto \begin{cases} (x_1 - 1, t - 1) [\text{prob. } p_+ = \epsilon(1 - a)] \\ (x_1, t - 2) [\text{prob. } p_0 = 1 - \epsilon] \\ (x_1 + 1, t - 1) [\text{prob. } p_- = \epsilon a] \end{cases} \quad (x_2, t) \mapsto \begin{cases} (x_2 - 1, t - 1) [\text{prob. } p_- = \epsilon a] \\ (x_2, t - 2) [\text{prob. } p_0 = 1 - \epsilon] \\ (x_2 + 1, t - 1) [\text{prob. } p_+ = \epsilon(1 - a)] \end{cases} \quad (\text{S40})$$

The probability that they annihilate (i.e. cross for the first time) at time τ is given by a sum over loops as in Fig. S4(a). It is easy to see that such loops are in one-to-one correspondence with a type of generalized *Motzkin walks* for the

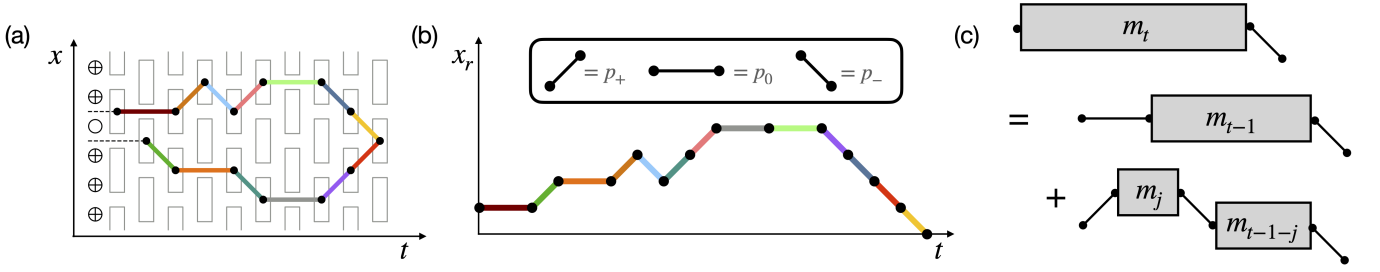


FIG. S4. Random walk picture for the relaxation of Pauli density with gate dilution ($\epsilon < 1$). (a) Random walks for the two endpoints $x_{1,2}$ of the \bigcirc domain. Rectangles represent gates in the brickwork circuit; walkers may only hop when on a gate. (b) Generalized Motzkin walk for the relative coordinate $x_r = x_2 - x_1$. Steps are color-coded to match (a). The three possible steps ($\delta x_r = \pm 1, 0$) have probabilities p_{\pm}, p_0 . (c) Diagrammatic representation of the recursion relation Eq. (S41) for the first-return probability (summation over $j = 0, \dots, t-1$ is implied).

relative coordinate $x_r \equiv x_2 - x_1$, where the flat step ($\delta x_r = 0$) covers two time steps ($\delta t = 2$) unlike the conventional Motzkin walks where all three possible steps have $\delta t = 1$. One such walk is shown in Fig. S4(b); it describes the evolution of the relative coordinate in Fig. S4(a).

We denote the probability of annihilation at time $2t+1$ by $p_- m_t$ (it is convenient to factor out the last step, which is necessarily $\delta x_r = -1$, hence the p_-). Then, we have $m_0 = 1$ and the Motzkin-like recursion relation

$$m_t = p_0 m_{t-1} + p_+ p_- \sum_{j=0}^{t-1} m_j m_{t-1-j}, \quad (\text{S41})$$

The idea is that the first step in the walk can either be $\delta x_r = 0$, or $\delta x_r = +1$. The former gives $p_0 m_{t-1}$ (as after the flat step, the problem remains unchanged up to $t \mapsto t-1$). In the latter case, the walk must at some point return to $x_r = 1$ (en route to $x_r = 0$); letting $2(j+1)$ be the time of first return to $x_r = 1$ (note this must be even), we obtain a term $p_+ m_j p_- m_{t-1-j}$. This is illustrated diagrammatically in Fig. S4(c). Finally one must sum over all possible values of j , obtaining Eq. (S41). We solve the recursion numerically and extract the scale $\gamma(\epsilon)$ from $e^{-\gamma(\epsilon)t} \sim m_t$.

We note that the result depends on p_+ and p_- only through their product $p_+ p_- = [\epsilon q / (q^2 + 1)]^2$. The purity calculation, Eq. (S39), has $p_+ = p_- = \epsilon q / (q^2 + 1)$, giving the same value for the product $p_+ p_-$. It follows that the return probability is the same in the two cases. Furthermore, in the purity calculation the random walk is unbiased ($p_+ = p_-$), so that up to a power-law correction the return probability is the same as the total survival probability; the latter is what maps onto the purity, $\sim q^{-v_E t}$. Adjusting for the fact that the computation of γ involves two random walks (for the left and right endpoints on the \bigcirc domain, Fig. S4(a)), or equivalently one Motzkin walk of doubled length (Fig. S4(b)), we obtain $e^{-\gamma t} \sim q^{-2v_E t}$ and thus $\gamma = 2 \ln(q) v_E$.

S6. DETAILS ON IMPS NUMERICAL SIMULATIONS

Here we present details of the computational method for simulating the dynamics of $p_{\mathbf{n}}$ under the averaged twirling circuit.

We use an infinite matrix product state (iMPS) description of $p_{\mathbf{n}}$. Due to the brickwork structure of the twirling circuits, this iMPS has a unit cell of two sites; thus

$$p_{\mathbf{n}} = \sum_{\alpha} \prod_i A_{\alpha_i, \alpha_{i+1}}^{n_i} B_{\alpha_{i+1}, \alpha_{i+2}}^{n_{i+1}} \quad (\text{S42})$$

in terms of tensors A, B of dimension $(2, \chi_1, \chi_2)$ and $(2, \chi_2, \chi_1)$ respectively, with $\chi_{1,2} \leq \chi$ for some fixed maximum bond dimension χ .

In order to obtain the shadow norm of a length- k fully packed Pauli string, we could start with an initial state $p_{\mathbf{n}}^{\text{init}} = \prod_{i \in R} \delta_{n_i, 1} \prod_{i \notin R} \delta_{n_i, 0}$, evolve it over t steps, contract it with the final boundary condition $f_{\mathbf{n}} = (q+1)^{-\sum_i n_i}$, and repeat for each value of k . A more efficient alternative is to instead start with the final boundary condition $f_{\mathbf{n}}$, which is trivially expressible as an iMPS with bond dimension $\chi = 1$ and tensors $A_{\alpha\beta}^n = (q+1)^{-n}$ (with dummy indices $\alpha = \beta = 1$) and $B = A$; evolve the iMPS “backwards” for t steps, i.e. under \mathbb{M}_t^T ; and then compute the shadow norm for all values of k at once.

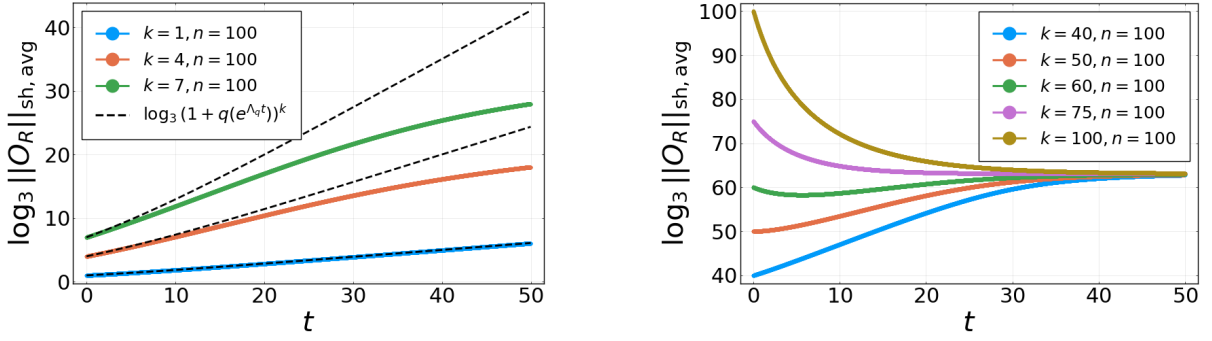


FIG. S5. Results for the shadow norm in the Brownian circuit model, from numerical integration of Eq. (S45) for a system of $n = 100$ qubits. (a) Few-body Pauli operators, $k \ll n$: the optimal depth is $t^* = 0$. (b) Large Pauli operators: the optimal depth becomes nonzero when the initial density k/n exceeds a finite fraction.

The evolution of the iMPS proceeds as follows. Under even layers of the twirling circuits, tensors A and B are merged by the action of an averaged gate $M = (1 - \epsilon)I + \epsilon M_{\text{Haar}}$, as in Eq. (S12). The tensor contraction reads

$$C_{\alpha_i, \alpha_{i+2}}^{m_i, n_{i+1}} = \sum_{m_i, m_{i+1}, \alpha_{i+1}} (M^T)_{m_i, m_{i+1}}^{n_i, n_{i+1}} A_{\alpha_i, \alpha_{i+1}}^{m_i} B_{\alpha_{i+1}, \alpha_{i+2}}^{m_{i+1}} \quad (\text{S43})$$

We then split C into two tensors A' and B' of bond dimension at most χ in the standard way (by performing a singular-value decomposition and keeping the largest 2χ values). This defines an update procedure $A, B \leftarrow f(A, B)$. Under odd layers of the twirling circuit, we simply have $B, A \leftarrow f(B, A)$. We iterate these two steps a total of t times ($t/2$ each).

Finally, to compute the shadow norm of a Pauli string of size k , we must contract the backwards-evolved iMPS with

an initial condition $|\cdots \circ \circ \overbrace{\bullet \bullet \cdots \bullet \bullet}^k \circ \circ \cdots \rangle$. To this end, we compute the left and right “environments” by finding the leading left- and right-eigenvectors of the transfer matrix $\mathbb{T}_{\alpha\beta}^\circ \equiv \sum_{\kappa} A_{\alpha\kappa}^0 B_{\kappa\beta}^0$. $\mathbb{T}_{\alpha\beta}^\circ$ has a unique unit eigenvalue (associated to the conservation of total probability under the stochastic dynamics); we label the corresponding left- and right-eigenvectors E_l, E_r . The shadow norm is then given by

$$\|O_A\|_{\text{sh, avg}}^2 = \langle E_l | \left(\mathbb{T}^{\bullet} \right)^{k/2} | E_r \rangle \quad (\text{S44})$$

where $\mathbb{T}_{\alpha\beta}^{\bullet} = A_{\alpha\kappa}^1 B_{\kappa\beta}^1$ and we assumed k even for simplicity. Note that the results for all values of k can be computed in one “sweep”, by computing the environments $E_{l,r}$ once and diagonalizing the transfer matrix $A^1 B^1$.

S7. RESULTS ON BROWNIAN CIRCUIT

Here we consider the time evolution of the weight distribution function (Eq. (3) of main text) under a “Brownian circuit”, see for example Refs. [60–62] for introductions to such models. The system we consider has n qudits undergoing random pairwise unitary gates. Specifically, within each “update step” with probability ϵ we apply a random unitary gate on a pair of randomly chosen qudits, and with probability $1 - \epsilon$ we do nothing. Here the parameter ϵ is the same dilution constant introduced in the main text for 1d circuits. A “time step” consists of n such update steps, to be comparable with finite dimensional circuits.

Within this model, the weight distribution function $\pi_w(t)$ evolves under the following master equation,

$$\frac{d\pi_w(t)}{dt} = \frac{n\epsilon}{\binom{n}{2}} \left\{ \frac{(q^2 - 1)^2}{q^4 - 1} [(w - 1)(n - w + 1)\pi_{w-1} - w(n - w)\pi_w] + \frac{2(q^2 - 1)}{q^4 - 1} \left[\binom{w+1}{2} \pi_{w+1} - \binom{w}{2} \pi_w \right] \right\}. \quad (\text{S45})$$

The operator weight can either increase or decrease under random unitary gates, as captured by the first and second term, respectively. For the relaxation of a single Pauli operator of weight k , as considered in the main text, we set the initial condition $\pi_w = \delta_{w,k}$.

We first focus on the early time dynamics with circuit depth at most $O(k)$, and for operator weight $k \ll n$. The equation is greatly simplified in this regime, as it suffices to focus on π_w with $w \ll n$,

$$\frac{d\pi_w(t)}{dt} = \Lambda_q [(w-1)\pi_{w-1} - w\pi_w], \text{ where } \Lambda_q = \frac{(2\epsilon)(q^2-1)}{q^2+1}. \quad (\text{S46})$$

The generating function of $\pi_w(t)$, defined as $f(z, t) = \sum_{w=0}^{\infty} \pi_w(t) z^w$, evolves under the following partial differential equation

$$\frac{\partial f(z, t)}{\partial t} = \Lambda_q z(z-1) \frac{\partial f(z, t)}{\partial z}, \text{ with initial condition } f(z, t=0) = z^k, \quad (\text{S47})$$

from which we obtain

$$f(z, t) = \left(\frac{ze^{-\Lambda_q t}}{1 - z(1 - e^{-\Lambda_q t})} \right)^k. \quad (\text{S48})$$

Finally, comparing with Eq. (2), we can immediately read off λ_A from $f(z, t)$,

$$\lambda_A = f(z = (1+q)^{-1}, t) = \left(\frac{1}{1 + qe^{\Lambda_q t}} \right)^k, \quad (\text{S49})$$

which is a monotonically decreasing function. In Fig. S5(a) we plot $\|O_A\|_{\text{sh,avg}} = \lambda_A^{-1}$ for $k \ll n$, from numerical solutions of Eq. (S45) at $q = 2$, and find good agreement. The optimal circuit depth is thus at $t^* = 0$, as consistent with the absence of comparable boundary and bulk effects.

On the other hand, when $k = O(n)$, λ_A can exhibit different behaviors depending on the operator density k/n , as we observe in Fig. S5(b). When $k/n < 1/2$, the boundary operator growth always dominates over the bulk operator relaxation, resulting in a monotonically increasing $\|O_A\|_{\text{sh,avg}}$, much like the case $k \ll n$. When $k/n > 1 - 1/q^2$, the operator density is above its equilibrium value, and the bulk relaxation process always dominates. When $1/2 \lesssim k/n \lesssim 1 - 1/q^2$, λ_A is non-monotonic, where the two effects are comparable at early times.